Journal of The Electrochemical Society

The Electrochemical Society
Advancing solid state & electrochemical science & technology

OPEN ACCESS

Silicene Anodes for Lithium-Ion Batteries on Metal Substrates

To cite this article: Alexander Y. Galashev and Ksenia A. Ivanichkina 2020 *J. Electrochem. Soc.* **167** 050510

Journal of The Electrochemical Society, 2020 **167** 050510

Silicene Anodes for Lithium-Ion Batteries on Metal Substrates

Alexander Y. Galashev[1,2,z] **and Ksenia A. Ivanichkina**[1]

[1] *Institute of High-Temperature Electrochemistry, Ural Branch, Russian Academy of Sciences, Yekaterinburg 620990, Russia*
[2] *Ural Federal University, Yekaterinburg 620002, Russia*

This article discusses heterogeneous materials containing silicene, which can be a promising anode for lithium-ion batteries. In addition to the current collector on an ultrathin insulator, the anode includes sheets of silicene spaced 0.75 nm apart. One of these sheets is on a metal substrate. Using the molecular dynamics method, we study new anode materials obtained from silicene on various metal substrates. In terms of the degree of filling of the anode and its mechanical strength, preference is given to Ni (111) and Cu (111) substrates. The highest degree of crystallinity of the packing is realized in a silicene channel on an Ag (111) substrate. The smallest local normal stresses appear in the channel walls on the Al (111) substrate. The voltage profile is defined as a function of the concentration of Li adsorbed on a two-layer silicene. The charge capacity of a two-layer freestanding silicene was estimated based on the study of its local destruction. Each of the considered metal substrates has a significant effect on the electronic properties of single-layer silicene, which leads to its metallization. The calculated partial densities of the electronic state allow us to establish the causes of the occurrence of metallic conductivity in silicene.

 [DOI: 10.1149/1945-7111/ab717a]

Manuscript submitted October 17, 2019; revised manuscript received January 14, 2020. Published February 11, 2020. *This paper is part of the JES Focus Issue on Heterogeneous Functional Materials for Energy Conversion and Storage.*

So far no natural layered silicon has been discovered, whose structure was similar to that of graphite. However, thin silicon films consisting of one or more atomic layers were obtained by depositing Si atoms on some metal surfaces.[1–4] In particular, the hexagonal symmetry of the Ag (111) surface favors the production of a single-layer two-dimensional silicon formed by hexagonal cells.[5] Such a film was called silicene. The existence of silicene was proved by the presence of certain electronic properties in it, also inherent in graphene. In particular, a linear dispersion was discovered for silicene at points K, K' of the Brillouin zone.[6] As is known, silicon is characterized by a high theoretical specific capacity (4200 mAh g^{-1}) and can be considered as the main candidate for use as an anode material for lithium ion battery (LIB).[7] However, crystalline silicon has a strong change in volume during cycling, because of which it is rapidly destroyed. Silicene is free from such a drawback and its use for the manufacture of the LIB anode seems promising. Single layer silicene obtained by epitaxial growth cannot be separated from the substrate. However, the layers of bilayer silicene can be separated, because Van der Waals forces act between Si atoms belonging to different layers. The metal substrate has a significant effect on the electronic properties of single layer silicene. As a rule, such silicene acquires metallic properties. An increase in the electronic conductivity of silicene favors its use as an anode material.

The Li^+ ion, which enters crystalline silicon, chooses a winding path for diffusion corresponding to the smallest radius of the valence orbital in Si.[8] In other words, the diffusion of Li into crystalline Si is anisotropic with a high degree of tortuosity of the path. On this path, the ion quickly gets an electron, becoming an atom. All subsequent time, an atom diffuses in silicon, not an ion. In graphite, the lifetime of the Li^+ ion is much longer. In particular, this is facilitated by the fact that the ionization potential of the C atom is almost 1.4 times greater than that of the Si atom. The radius of the C atom is 1.8 times smaller than the radius of the Si atom. As a result, during the transition from silicon to carbon, the distance between a pair of nuclei decreases. The overlap of the p-orbitals of two carbon atoms occurs much more efficiently due to the shorter distance between the nuclei. Therefore, the total electronic structure of the solid carbon material is much more stable than for the corresponding silicon material. The electron transfer to the Li^+ ion in the carbon material is difficult.

When a lithium-ion battery is charged, lithium ions pass through an electrolyte and, upon reaching a silicon electrode, combine with electrons to form lithium atoms.[9] This process occurs at the interface between the electrolyte and the surface Li_xSi. This is facilitated by a higher electronic conductivity than silicon of the Li_xSi compound. Li atoms diffuse over the silicon volume, not ions. At the same time, diffusion of lithium ions in graphite was proved experimentally.[10]

The energy aspect of the electron-ion interaction in functioning metal-ion batteries were considered in[11] based on the electrochemical model of the semiconductor, which allows a better understanding of the interface (electrolyte/active material and active material/substrate) effects. In the proposed model, the driving force of the reaction is represented as a change in the Fermi energy due to a compromise between the electron and ion concentrations in the interface region. So far, it has not been possible to solve the problem of the formation of a solid electrolyte interphase (SEI). This phenomenon in ion batteries with a metal Li anode was studied in,[12] where the thermodynamic aspect of the appearance of Li dendrite was also considered. SEIs are also formed in LIBs using both liquid and solid electrolytes. Various methods can be used to block the formation of Li dendrites. Dendrite growth was considered in the framework of the film growth model based on the study of surface energy. The nature of the film growth depends on the difference in surface energy between the substrate and the film, as well as on the mismatch of the lattices of the film and the substrate. The high surface energy of the anode material stimulates the suppression of lithium dendrites during charge/discharge cycles. The formation of lithium dendrites in LIB is unlikely. However, the currently used LIBs do not satisfy the growing need for high energy density and need improvement.

In the present work, a channel formed by two sheets of silicene is considered as an anode element. The channel was located on various metal substrates (Ag, Al, Ni, and Cu). For the considered element of the anode, the processes of intercalation and deintercalation of Li^+ ions were studied by molecular dynamics (MD). In addition to the influence of the substrate material on the passage of these processes, we also study the role of defects on the strength of the channel walls and on its fillability with lithium.

The purpose of this work is to consider the possibility of using a two-layer silicene, which has defects and is located on various metal substrates, as the material of the anode of a lithium-ion battery.

[z] E-mail: galashev@ihte.uran.ru

Computer Model

Sheets of silicene with a floral structure[13] were arranged horizontally one above the other. The unit cell of silicene had a rhombic shape and contained 18 atoms, six of which were elevated relative to the basal plane.[14] The gap h_g between the sheets was selected empirically and amounted to 0.75 nm. With such a gap, lithium atoms could rather freely diffuse along the channel.[15] The channel formed by silicene sheets was located on any of the metal (Ag, Al, Ni, and Cu) substrates. The crystalline substrates were facing the channel with the (111) face. The channel did not have material sidewalls. However, it was surrounded by an artificial force barrier, which made it difficult for atoms to escape through the side and back surfaces.[16] Through the entrance (frontal surface), Li^+ ions were periodically introduced into the channel with an interval of 10 ps. Ions were introduced either in pairs or singly, and were "drawn" into the channel due to the applied electric field having a voltage of 10^3 V m^{-1}. After 10 ps, the Li^+ ion entering the channel turned into a lithium atom,[16] which subsequently did not "feel" the presence of an electric field.

The schematic diagram of the electrochemical cell for LIB considered in this work is shown in Fig. 1. The anode (left) includes a current collector (thin Cu film), an insulator, and two sheets of silicene, one of which is located on a metal (Ag, Al, Cu, Ni) substrate. Metal substrate and sheets of silicene are isolated from both electrodes. The upper silicene sheet does not have a metal substrate, which makes it possible to use both sides of this sheet when constructing the LIB. LIB can be obtained by joining in the vertical direction of such cells. It is more advantageous to connect mirrored elements (relative to a plane parallel to the plane of silicene). In this case, in principle, for two sheets of silicene (without support), each of the surfaces can be used for lithium adsorption. Silicene sheets are separated by a gap of 0.75 nm using a solid electrolyte (right). On the left they rest on the insulator. The cathode (right) is in direct contact only with solid electrolyte. When charging the battery, Li^+ ions fill the silicene channel (anode element), and when discharged through a solid electrolyte, they partially return to the cathode. The structure of the electrolyte and the cathode material is not considered here. The types of solid-state electrolytes and the prospects for their use are discussed in.[17] High-energy cathodes with high chemical resistance for lithium-ion batteries are discussed in.[18] The external electric circuits are conventionally shown. In real conditions, the discharge of the battery is accompanied by a decrease in voltage between its electrodes. Molecular dynamic modeling of such a process requires an extremely large amount of computer time. The total duration of all the calculations was about 250 million time steps, i.e. ~25 ns. Therefore, the discharge process was simulated by us at a constant value of the voltage at the electrodes, i.e. at a constant value of the intensity of the reverse direction stronger electric field.

At low electrical voltages (less than several tens of volts), the gap between the elements of the conductive pattern of the printed circuit board in critical places should be at least 0.1 mm. The gap of 0.75 nm is 7.5 10^5 times less than this value. Having an initial zero velocity in vacuum in an electric field of intensity 10^4–10^5 V m^{-1}, the electron will fly a distance of 0.75 nm in 0.92–0.29 ns. Such a gap guarantees the passage of electrons through the silicene channel even in vacuum at a voltage of ~1.5 V. As will be shown below, silicene on a metal substrate acquires electrical conductivity and is not an obstacle to the transfer of electrons to lithium. Consequently, there is practically no interference for electrons in order to reach lithium ions during battery charging and to take away electrons from lithium during its discharge. Currently, an industrially produced metal foil that can be used to support silicene has a minimum thickness of 20 nm. Thin-layer multilayer samples $(ZnO/SiO_2)_{25}$, consisting of layers of nanocrystalline ZnO and interlayers of amorphous SiO_2, with a bilayer thickness of 6 to 10 nm at a temperature of <580 °C, have a specific electrical resistance 140 times greater than a thin Ni film and 620 times larger than the Ag

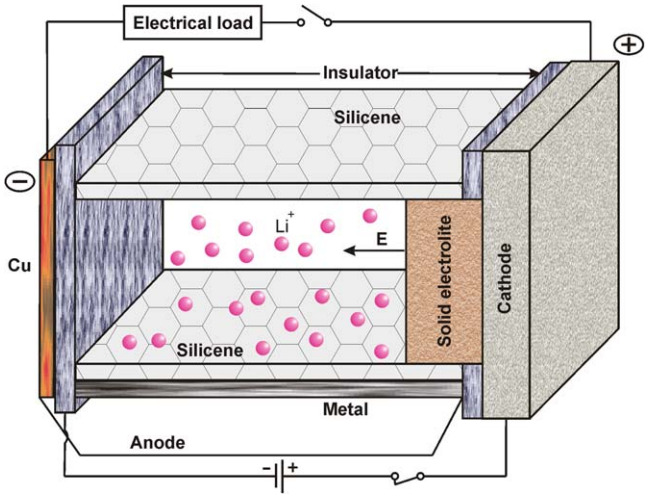

Figure 1. Schematic diagram of a cell of a lithium-ion battery with a silicene anode.

film.[19] Therefore, even such isolation is enough to separate the cathode from the anode in a miniature LIB. When charging the battery (the external circuit is closed), the current passes through a metal foil, and not through an insulating film.

The walls of the channel were represented either by sheets of perfect silicene or silicene containing defects. The sheet size was 4.8 × 4.1 nm. Nine defects were approximately evenly distributed on each of the sheets of silicene. Defects were mono-, bi-, tri-, and hexavacancies. Si atoms located along the perimeter of both sheets of silicene were immobile during all calculations, but interacted with other (mobile) Si atoms and atoms of the metal substrate, as well as with lithium atoms (ions). Thus, the gap at the entrance to the silicene channel and at the exit from it remained unchanged during the simulation.

The ion injection procedure was carried out until the channel was completely filled with lithium. When the limit was reached, the ions could no longer enter the channel and moved already beyond it. Deintercalation began by reversing the direction of the electric field vector, and the field strength increased to 10^5 V m^{-1}. The ion or pair of ions that entered the channel last was the first to start the deintercalation process. Then, their intercalation precursors became ions. Under the influence of an electric field, they were removed from the channel. This process continued until the channel was empty.

The interaction between Si atoms located in the same silicene sheet was carried out using the Tersoff potential.[20] To describe the interaction between metal atoms in the substrate, the embedded atom potential (EAM) was used.[21] Cross interactions, including the interaction between Si atoms belonging to different sheets of silicene, were carried out on the basis of application of the Morse potential.[22–24] If two ions were simultaneously present in the channel, there was a Coulomb interaction between them as an addition to the interatomic interaction used.

The self-diffusion coefficient of lithium atoms in the silicene channel was determined as

$$D = \lim_{t\to\infty} \frac{1}{2\Gamma t}\langle[\Delta\mathbf{r}(t)]^2\rangle, \qquad [1]$$

where Γ is the dimension of space, $\langle[\Delta\mathbf{r}(t)]^2\rangle$ is the mean square of the displacement of atoms, $\langle ... \rangle$ denotes the averaging of the considered quantity over time.

The stress distribution in the sheets of silicene was investigated as follows. The silicene sheet was divided into elementary areas elongated along the "armchair" or "zigzag" directions and having the normal γ (x, y, z). During intercalation (deintercalation), the resulting force acting on each elementary area was calculated.

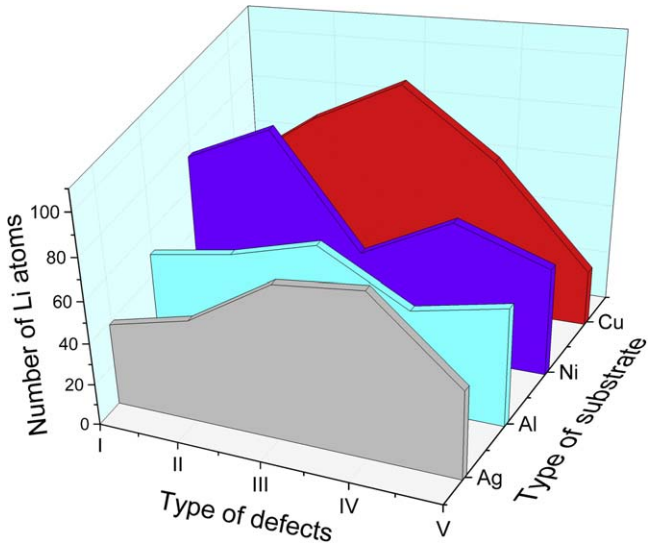

Figure 2. Limit number of Li atoms intercalated into silicene channels located on Ag, Al, Ni, and Cu substrates. I—channel made of perfect silicene, II–V—channel walls made of silicene with mono-, bi-. three- and hexavacancies, respectively.

When determining the resulting force, only those interactions between i and j atoms were taken into account for which the force vector passed through the area under consideration.[25] In addition, when calculating $\sigma_{\gamma\alpha}(l)$, the direction α (x, y, z) of the velocities of i and j atoms was taken into account:

$$\sigma_{\gamma\alpha}(l) = \left\langle \sum_{i}^{n} \frac{1}{\Omega}(m v_{\gamma}^{i} v_{\alpha}^{i}) \right\rangle + \frac{1}{S_l} \left\langle \sum_{i}^{n} \sum_{j \neq i}^{(u_i \leqslant u, u_j \geqslant u)} (f_{ij}^{\alpha}) \right\rangle, \qquad [2]$$

The following notation is used in expression 2: n is the number of atoms on the l-area, Ω is the volume per atom, v_{α}^{i} is the α-projection of the velocity vector of the atom i, S_l is the area of the l area, m is the mass of the atom, f_{ij}^{α} is the α-projection of the resulting force between i and j atoms, the vector of which penetrates the l-area, u_i is the current coordinate of the i atom, in the upper index of the sum u denotes the coordinate of the meeting point of the line passing through the centers of the atoms i and j with l-area.

The analysis of lithium packings in the channel was carried out using the construction of Voronoi polyhedra (VP). One of the main characteristics of this structure research method is the angular distribution of the nearest geometric neighbors. The angle θ is considered, the vertex of which coincides with the center of the VP, and the sides pass through this vertex and the centers of two atoms included in the number of nearest neighbors.

The adhesion energy between the metal substrate and the silicene sheet was determined according to the expression:

$$E_{\text{adh}} = \frac{E_{\text{tot}} - E_{\text{Me}} - E_{\text{Si}}}{n} \qquad [3]$$

where E_{tot} is the total energy of the entire system, E_{Me}, E_{Si} are the energies of the metal substrate and silicene, respectively, and n is the number of atoms in the system.

Lithium interacts with silicene more strongly than with graphene.[26] Therefore, silicene is able to retain a larger number of lithium ions than graphene, and, therefore, it can be expected that it also has a large charge capacity. To determine the maximum concentration of lithium adsorbed on silicene and not destroying the Si–Si bond, we performed a separate molecular dynamic calculation. We studied bilayer silicene with a gap between the sheets $h_g = 0.75$ nm. Silicene had a package represented by a 4×4 supercell of 18 atoms.[14,27] Each sheet of silicene contained 54 atoms. The sheets were arranged one above the other parallel to the xy plane. The size of the silicene sheet, taking into account the size of the Si atoms, was 1.90×2.25 nm. Silicene was placed in a rectangular box with impermeable walls. Moreover, the distances between the extreme Si atoms and the box walls were approximately the same. Initially, the box was randomly filled with 300 Li atoms so that the minimum distance between the Li and Si atoms or Li and Li ones was not less than 0.27. Next, an MD calculation was carried out with a duration of 5 million time steps (step $\Delta t = 10^{-16}$ s). In this case, Li atoms filled the channel formed by silicene sheets and were adsorbed on the outer walls of the channel. Li atoms not bound to silicene directly or through other Li atoms were removed from the system. If individual Si atoms were removed from the sheet by a distance exceeding 0.27 nm (the length of the Si–Si bond in silicene is 0.228 nm), it was believed that silicene began to break down under the action of adsorbed Li atoms. The limiting Si–Si bond length of 0.28 nm was chosen in accordance with a relative critical strain of 0.182, which leads to the destruction of silicene during its uniaxial tension.[28] In this case, the MD calculation was performed again with each time the number of Li atoms reduced by 5. In the end, a configuration with non-destructible silicene was obtained, which was used as the initial one for DFT calculations. By x_2, we will denote the lithium concentration in the system preceding the one selected for the DFT calculations.

Further research to obtain the concentration dependence of the electric potential was based on DFT calculations using the SIESTA program.[29] The calculations were performed based on the theory of the density functional,[30] selected pseudopotentials,[31] and the generalized gradient approximation (GGA) in the form of Perdew, Burke, and Ernzerhof (PBE).[32] We used a basic set of plane waves and cutoff of kinetic energy at a level of 200 Ry. The Brillouin zone was set using the Monkhorst-Pack method using $10 \times 10 \times 1$ k-points.[33]

The system with non-destructible silicene obtained because of MD modeling was subjected to dynamic relaxation in the framework of the DFT model. Then, a certain part of randomly selected (starting from the outer sides of the bilayer silicene) Li atoms was removed from the system so that its concentration corresponded to the value, and dynamic relaxation of the system was again carried out. As a result, a system was obtained corresponding to the state achieved by partial deintercalation (the current state with lithium concentration x_1). The deintercalation process was divided into 10 parts, i.e. implemented 10 x_1 values. The procedures for finding the initial configuration with non-destructible silicene and performing the subsequent "deintercalation" were repeated three times with different random numbers corresponding to the arrangement of lithium atoms.

The dependence of the voltage generated by a silicene element on the concentration of lithium ions present in it is given by the expression[34]

$$V(x) = \frac{-[E_{\text{Lix2Si}} - E_{\text{Lix1Si}} - (x_2 - x_1)E_{\text{Li}}]}{(x_2 - x_1)e}, \qquad [4]$$

where, x_1 is the current lithium concentration in silicene and x_2 is the Li concentration corresponding to the initial filling of bilayer silicene, E_{Lix1Si} and E_{Lix2Si} is the energy of the "silicene-lithium" system at lithium concentrations x_1 and x_2, correspondingly, E_{Li} is the total energy of bulk lithium metal, e is the elementary electric charge.

Using the SIESTA program, we also calculate the density of states (DOS), which for a given band n is determined by the expression

$$N_n(E) = \int \frac{d\mathbf{k}}{4\pi^3} \delta(E - E_n(\mathbf{k})), \qquad [5]$$

where the disperse of the band enters the δ-function in the form of the argument $E_n(\mathbf{k})$, and the integral is taken over the Brillouin zone.

Qualitatively, the picture of creating DOS is revealed by calculating the corresponding partial spectrum (PDOS), which

shows which atoms in the system form certain electronic states. In addition, PDOS gives an idea of the presence of electron hybridization in the system. Since the main effect of the substrate is its effect on the sheet of silicene directly adjacent to it, PDOS calculation was performed for a single-layer silicene. The metal substrate was defined by 147 metal atoms (Al, Ni, Cu, Ag) located in three layers. A silicene sheet on this substrate contained 54 atoms.

For parallel computations, the standard LAMMPS code was used, which was developed for classical MD modeling.[35] The code was supplemented with fragments allowing calculating the kinetic and mechanical properties of the system. All calculations were performed on a URAN cluster-type hybrid computer at the IMM UB RAS with a peak capacity of 216 Tflop/s and 1864 CPU.

Results

In this study, we selected the best metal substrate for the channel, as well as searched for the optimal size of defects in silicene at which the channel is maximally filled with lithium. Figure 2 shows the ultimate occupancy of a silicene channel with lithium when the channel is located on various metal substrates. The type of substrate is one of the parameters, and the other parameter is the type of defects. Defects are indicated by Roman numerals. The highest occupancy was obtained for a channel with monovacancies if it was on a Ni (111) substrate, as well as for a channel with bivacancies when it was placed on a Cu (111) substrate.

The self-diffusion coefficient D of lithium atoms in the channels on different metal substrates is of the order of $\sim 10^{-5}$ cm^2 s^{-1}, i.e., it seems to be a large value. This is an encouraging result, as a large value of D should lead to a high battery charging speed. The coefficient D turns out to be a strongly fluctuating quantity when considering its dependence on the number of lithium atoms present in the channel. Figure 3 reflects the behavior of the coefficient D during cycling for channels located on the Ni (111) substrate. As a rule, at the initial stage of intercalation, fluctuations D are large due to the transient nature of the process. The size of fluctuations D in channels with defects usually decreases at the final stage of deintercalation due to a decrease in the number of collisions between lithium atoms. However, in the channel with perfect silicene walls, such a decrease in the fluctuations of D is not observed due to the enhanced collisions of lithium atoms and ions with the walls at the final stage of deintercalation.

When the channel is filled with lithium, stresses appear in the channel walls. Strong stresses can destroy the walls. Therefore, it is important to know the stress distribution along the channel in different directions. Figure 4 shows the distribution of stresses normal to the walls of the channel when moving along the channel in the direction of "chair." Here stresses in the walls of a monovacancies silicene channel located on four different metal substrates are shown. It is seen that in the presence of a copper substrate, the most intense stresses develop in silicone; while in the presence of an aluminum substrate, these stresses are minimal. However, even in the case of a copper substrate, the maximum local stress does not exceed 44% of the tensile strength of silicene under uniaxial tension.

Figure 5 shows the xy-projections of the lower silicene sheet together with the corresponding projections of Li atoms falling into the lower half of the space separated by a horizontal plane at the level $h_g/2$. The figure shows the bonds between Si atoms to highlight defects. It can be seen that all defects (bivacancies) retain their initial shape only on the Ni (111) substrate. However, among all the substrates under consideration, only on the Ag (111) substrate, silicene lost two extreme atoms during lithium intercalation. This is due to the low binding energy (0.41 eV) of silicene with this substrate, which, for example, is 2.1 times weaker than the binding energy between silicene and a Cu (111) substrate.[36] In this case, in the space adjacent to the lower silicene sheet there are 20 li atoms. In the case of an aluminum substrate, the number of Li atoms adjacent to the lower silicene sheet is 28, for a copper substrate −34, and for a nickel one −12. In the latter case (on a Ni substrate), the maximum number of Li atoms intercalated into the channel is achieved when defects in silicene sheets are monovacancies rather than bivacancies. Li atoms often occupy positions above the centers of hexagonal rings formed by Si atoms. Therefore, a partially regular packing of lithium atoms forms in the channel. In the channel on the Ni (111) substrate, all nine bivacancies retained their original shape. Six bivacancies retained their original shape in a silicene sheet located on an Ag (111) substrate, five retained their shape close to the initial one on the Cu (111) substrate, and not a single bivacancy have retained its shape on the Al (111) substrate. Instead of the disappeared bivacancies, cyclic formations (including large ones) with a different number of links appeared. Thus, the distortion of the structure of the lower silicene sheet is amplified, passing from substrate to substrate in the sequence: Ni → Ag → Cu → Al. The same sequence of the degree of distortion of the shape of defects is preserved for the upper silicone sheet.

Using classical MD calculations, we obtained the following values of the cohesive energy between a metal substrate and a perfect silicene sheet: 0.89, 0.41, 0.85, and 0.34 for Ni, Ag, Cu, and Al, respectively. Thus, among the investigated substrates, nickel and copper ones have the strongest adhesion to the bottom sheet of perfect silicene.

Figure 6 shows the change in the channel volume upon filing with lithium (V_i) relative to the volume V_0 of the empty channel for various metal substrates. As can be seen from the Fig. 6, the largest increase in volume when filling the channel with lithium is, as a rule, observed when using an Ag (111) substrate. An exception is the channel, the walls of which contain hexavacancies. In this case, the relative increase in the channel volume on the copper substrate is the highest, but at the same time, silicene is destroyed. Earlier, we found that the most suitable anode material is silicene with mono- and bivacancies, i.e. silicene, having the type of defects II and III. The minimum change in channel volume for such types of material is achieved on a copper substrate, and for a channel with bivacancies, the volume change is negative. In this case, the channel decreases its volume due to the stronger attraction of the top sheet of silicene to the lithium filling the channel. The number of Li atoms in a completely filled channel on a copper substrate is maximized ($N_{\mathrm{Li}} = 86$) precisely for silicene with type III defects. Only the silicene channel with monovacancies (type II) on a nickel substrate was more fully filled ($N_{\mathrm{Li}} = 91$). However, the change in channel volume when using a nickel substrate is higher than for a channel on a copper substrate.

Using the statistical geometry method, the angular distributions of the nearest geometric neighbors for lithium packings in the channels are obtained. Figure 7 shows the θ distributions obtained for the walls of channels with bivacancies. Narrow, high peaks periodically placed in the angle range $0^\circ \leqslant \theta \leqslant 180^\circ$ reflect the degree of crystallinity of the packiges. The better the characteristic peaks are resolved, the closer the packing is to crystalline. It is seen that the greatest crystallinity is manifested by the packing of lithium in the channel on the silver substrate, and the worst—in the channel on the copper substrate.

The calculated voltage profile $V(x)$ created by the silicene element is shown in Fig. 8. In the region of low Li concentrations ($x < 1$), there is a small voltage fluctuation near 0.075 V. This may be due to significant, rapidly changing deformations of silicene sheets, as a result of which the energy $E_{\mathrm{Li}x\mathrm{Si}}$ also noticeably changes. This, in turn, entails some change in the magnitude of the voltage. In addition, there is a large selection of different sites for the deposition of Li atoms on silicene. The energy $E_{\mathrm{Li}x\mathrm{Si}}$ also depends on the place (for example, above the Si atom, or into the hole between the silicon atoms) where lithium ion is adsorbed. In other words, there are certain perturbations affected the definition of $V(x)$ that are not related to the value of x. The point on the graph corresponding to $x =$ 1.45 indicates the onset of silicene destruction. Bearing in mind that in the presence of chemical bonding in the "non-destructible" alloy, $\mathrm{Li}_x\mathrm{Si}$ x reaches a value of 4.4, it is possible to estimate the charge capacity when lithium is filling a freestanding two-layer silicene as

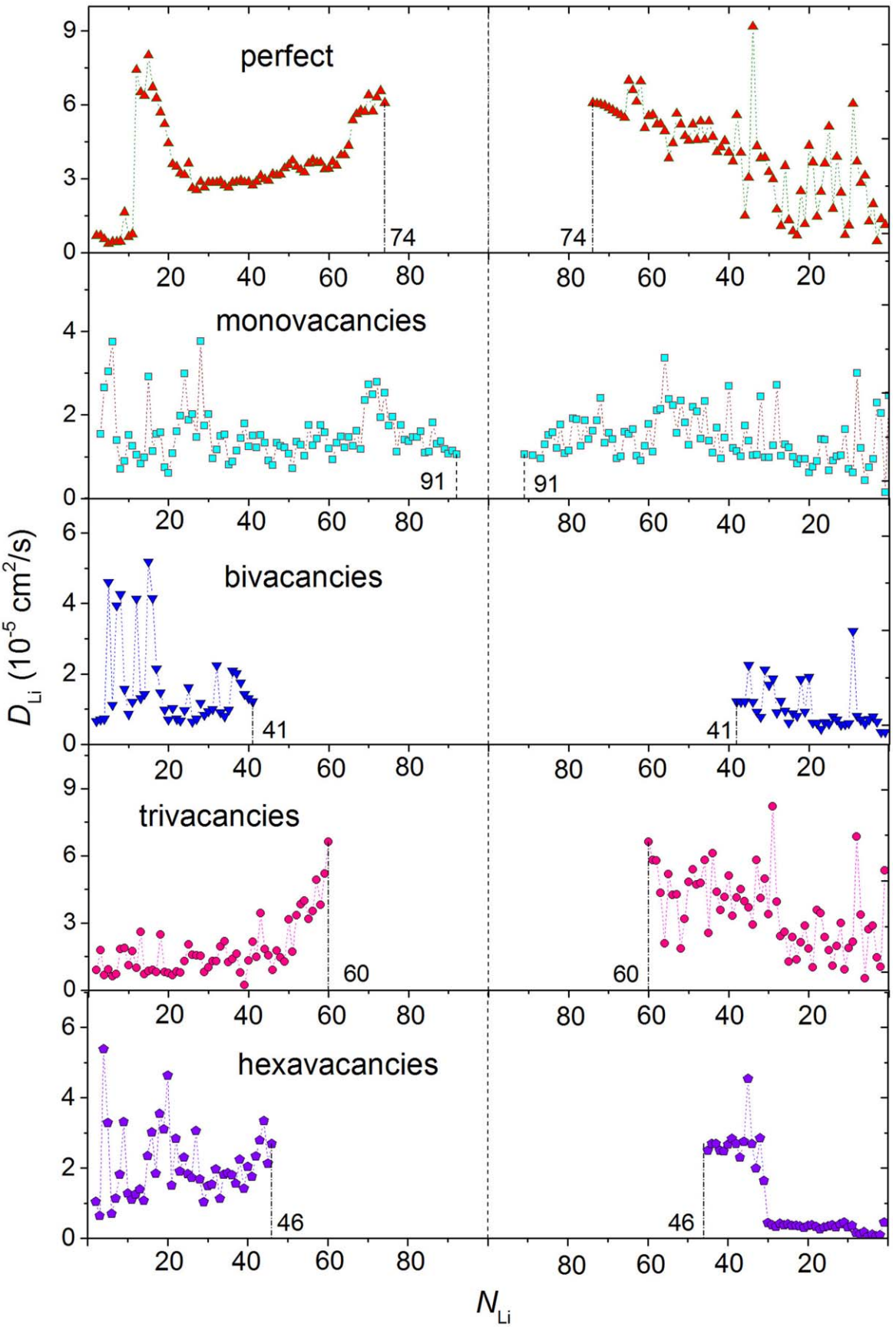

Figure 3. Self-diffusion coefficient of lithium atoms during intercalation (left) and deintercalation (right) in various silicene channels on a Ni (111) substrate. (a) perfect silicene, (b) silicene with monovacancies, (c) bivacancies, (d) trivacancies, and (e) hexavacancies. The maximum achievable number of lithium atoms in the channels is indicated by a dashed-dotted line.

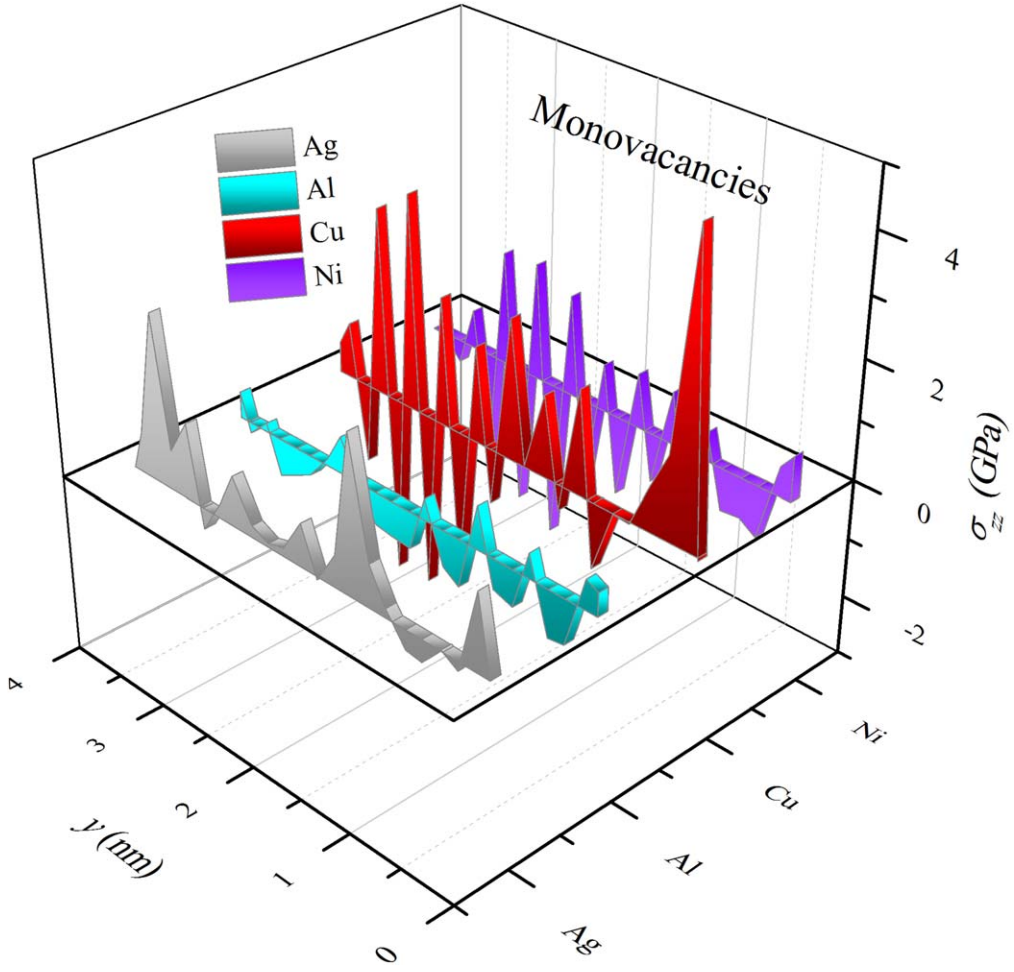

Figure 4. Distribution of average stresses σ_{zz} in sheets of silicene with monovacancies along the direction *oy* (armchair), when lithium is intercalated in silicene channels located on Ag, Al, Cu, and Ni substrates. Elementary areas are elongated along the axis *ox*.

1384 mA·h g^{-1}. This value is 13.6% higher than the similar value obtained for single-layer silicene.[34]

Partial electronic state spectra (PDOS) characterizing silicene in heterostructures of various nanocomposites are shown in Fig. 9. It can be seen that silicene acquires metallic conductivity on all considered substrates, which can be caused by various factors. On copper and silver substrates, p-d hybridization between silicene and metal is observed. A similar result was obtained for silicene on an Ag substrate in.[37] On an aluminum substrate, silicene acquires conductivity due to p-s hybridization between silicene and metal. The partial spectrum of electronic states of the system "silicene-Ni substrate" indicates the main contribution of the intrinsic p-electrons to the conductivity of silicene. Hybridization of orbitals in the conduction band for silicene and Ni is not observed. In this case, the metallic conductivity of silicene appears due to the close approach of the Si and Ni atoms, which leads to a significant decrease in the degree of corrugation of silicene. As a result, the ductility of silicene increases, which entails an increase in its electrical conductivity.

Discussion

At a concentration of $x = 1$, the $V(x)$ potential becomes negative. This implies a change in the adsorption mechanism, possibly with the appearance of Li–Li bonds and with the development of a tendency for the Si–Si bond to break. The sharp decline in the dependence $V(x)$ can also be associated with the appearance of a "phase" with a higher Li content ($x \geqslant 1$). Stepwise smoothing of the $V(x)$ dependence occurs during the formation of characteristic crystalline phases ($Li_{12}Si_7$, Li_7Si_3, $Li_{13}Si_4$, and $Li_{22}Si_5$) if intercalation in silicene is carried out at a higher temperature (688 K).[38]

Heterostructures based on silicene with pronounced metallic properties have already been obtained by replacing silicon with boron.[39] The two-dimensional structures of composition BSi_3 had a flat geometry and higher electronic conductivity than free-standing silicene. An assessment was made of the theoretical charge capacity of boron silicene. In the case of a single-layer BSi_3, it was 1410 mA·h g^{-1}, and the capacity of a two-layer BSi_3 was estimated as 846 mA·h g^{-1}. These estimates of the charge capacity are in qualitative agreement with our value for free-standing two-layer silicene. The metallization of silicene on a metal substrate is observed to increase the charge/discharge rate when using such an anode in the LIB.

As a rule, theoretical studies of physical properties are performed for freestanding silicene. This substance is useful for comparing the properties of silicene with graphene. An important difference between graphene and silicene is that freestanding graphene is a reality, while silicene does not exist in this state. Epithexially obtained silicene cannot exist outside the substrate on which it was obtained. This indicates that the substrate has a huge impact not only on stability, but also on the very existence of silicene. Therefore, the properties of real silicene are largely determined by the influence of the substrate. This can be shown in the following example. In the band structure of silicene, the existence of the Dirac cone was predicted.[36] The presence of this property suggests that the electrons near the Fermi level turn out to be massless, which leads to ultrahigh mobility of these charge carriers. Preservation of super

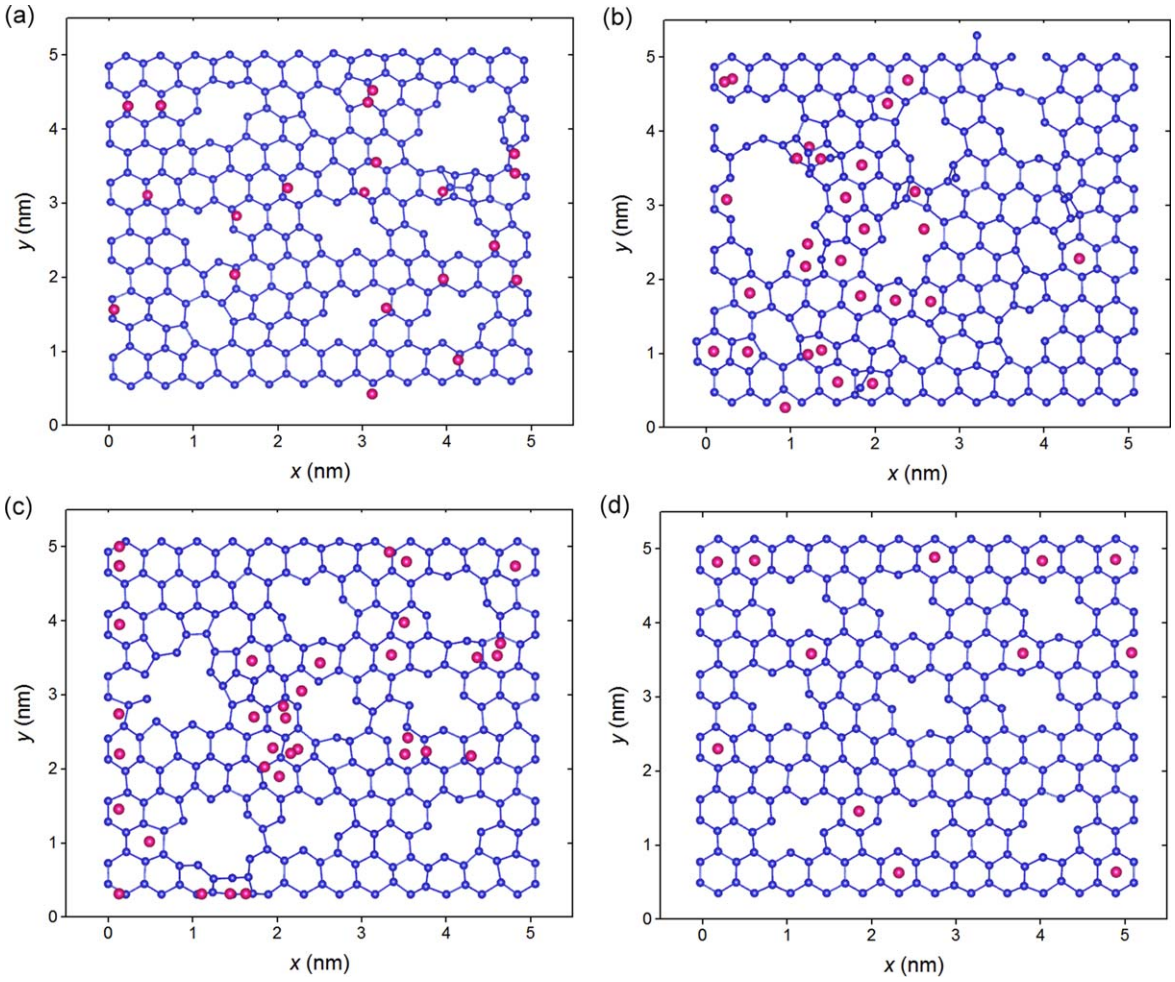

Figure 5. The *xy* projection of the lower silicene sheet, initially containing 9 bivacancies, with the channel positioned on: (a)—Al(111), (b)—Ni(111), (c)—Cu (111), and (d)—Ag(111) substrate at the time of complete lithiation; blue circles are Si atoms, red circles are Li atoms.

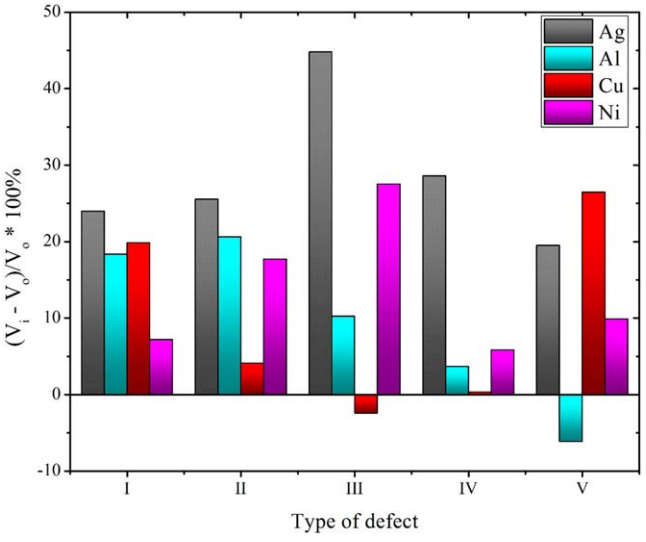

Figure 6. The relative change in the volume of the silicene channel during its maximum filling with lithium, when the channel walls are made: I—of perfect silicene or with II—mono-, III—bi-, IV—tri-, and V—hexavacancies.

high electron mobility is extremely important when using silicene in nanoelectronics. In the case of using silicene as an electrode material, this property can only be used indirectly, since the main charge carriers in metal-ion batteries are ions, not electrons. However, electrons are involved in chemical reactions taking place on electrodes. First-principle calculations showed that the Dirac cone is destroyed due to strong hybridization of the zones when silicene is on the substrates Ir, Cu, Mg, Au, Pt, Al, and Ag.[40] However, when the silicene channel is filled with lithium, as well as when lithium enters the gap between the metal substrate and silicene, the Dirac cone in its zone structure will be restored to a certain extent. The use of Ag, Cu, and Ir substrates gives strong hybridization with silicene located on them. The Dirac cone also collapses if silicene is on a ZrB2 substrate. Different metal substrates do not have the same effect on graphene. For example, because of chemisorption the Dirac graphene cone also breaks down on Ni, Co, Ti, and Pd substrates.[41] The reason for this is significant hybridization between the p_z orbital of graphene and the *d* orbital of the metal. Physiosorption of graphene on Al, Cu, Ag, Au, and Pt substrates does not lead to destruction of the Dirac cone in its band structure.[42] During the intercalation of Na, K, Cs, Al, Cu, and Au atoms in graphene containing systems, the strong interaction between graphene and the Ni (111) substrate weakens.[43]

As we have already noted, the critical length of the Si–Si bond was established in accordance with.[26] In this work, it was shown that under uniaxial tension in the zigzag direction brittle fracture is observed in silicene at 300 K. These calculations were performed using molecular dynamics with the MEAM potential. The ultimate strength was 13.9 GPa, and Young's modulus was 861 GPa. When the relative strain reached 0.182, a direct break of the Si–Si bond occurred. In this way, a small crack arose, which then developed

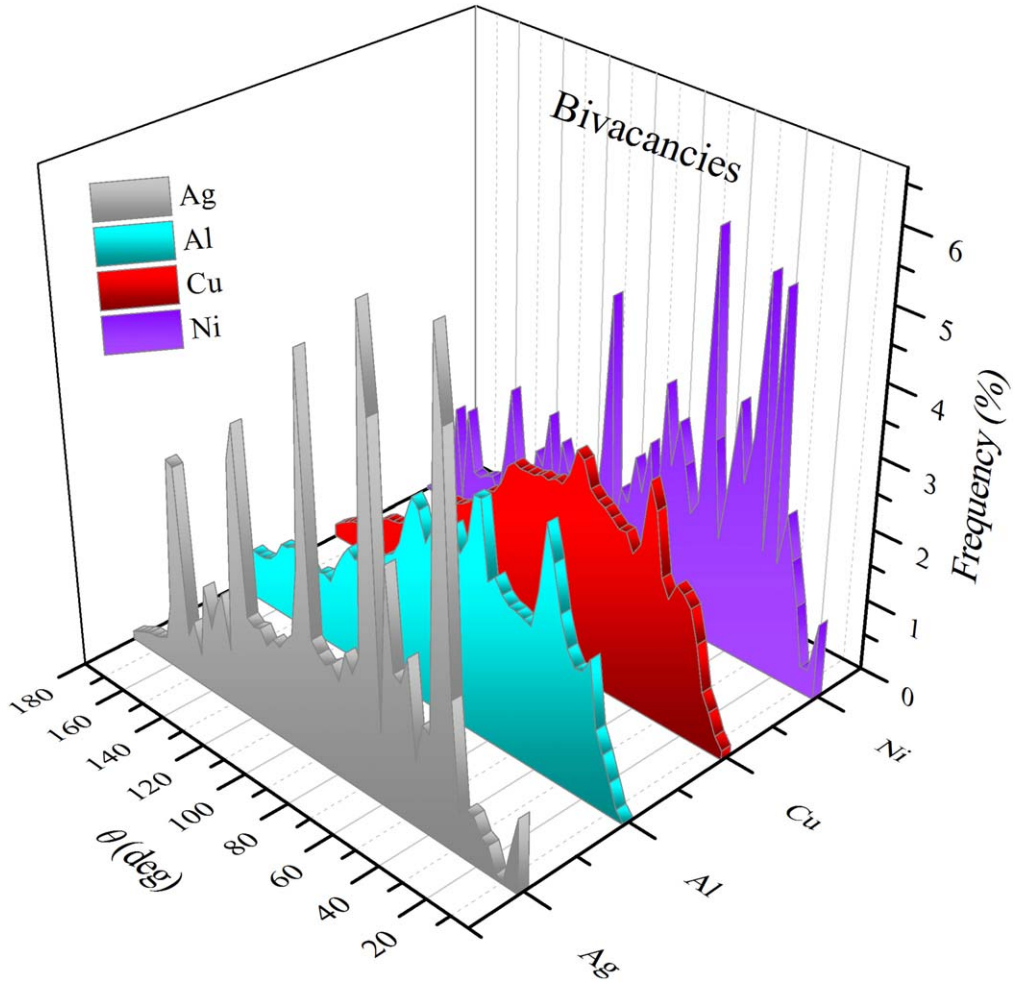

Figure 7. Angular distributions of the nearest geometric neighbors in lithium packings in silicene channels located on Ag, Al, Cu, and Ni substrates. The walls of the channels contain bivacancies.

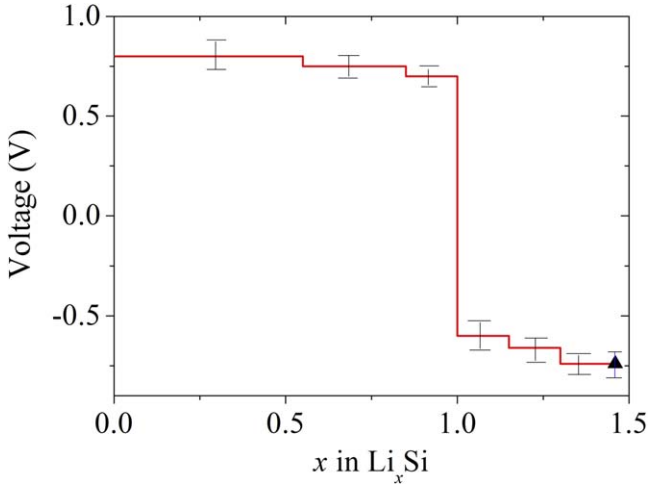

Figure 8. The calculated voltage profile as a function of the concentration of Li adsorbed on silicene. The errors in determining the voltage are shown by vertical segments. The point on the graph reflects the concentration $x = 1.45$, at which the destruction of silicene begins.

spontaneously and failure occurred without manifestation of ductility. The tensile strength and fracture strain of silicene were significantly higher than that of bulk silicon, and Young's modulus, on the contrary, was lower.

The strong interaction with the substrate is indicated by the presence of significant epitaxial stress in silicene.[44] The deposition of metal clusters can be accomplished by "soft landing" on solid Ar (111) over the desired substrate.[45,46] After metal deposition, the buffer layer of the solid noble gas is evaporated. Our study showed that the deposition of silicene on metal substrates such as [Ag, Al, Ni, Cu] (111) does not preserve the unique properties of silicene due to strong interfacial bonds. It is necessary to search for new substrates and create conditions under which silicon grows in two dimensions without three-dimensional aggregation. In addition, the bonds of Si with the substrate should be rather weak.

In the presence of a metal substrate, silicene passes from a narrow-gap semiconductor to a metal. This, together with low diffusion barriers of Li, suggests that silicene on a metal substrate has an increased charge/discharge rate.[47] The presence of such a property is essential for the use of heterogeneous functional materials in flexible metal-ion batteries.

The Tersoff interatomic potential provides a good description of the bulk and elastic properties of silicon. However, it tends to overestimate the barrier to brittle fracture of the crystal lattice, which leads to an overestimation of the viscosity of the system upon fracture.[48] The Morse potentials we use are based on the fit to the experimental values of the elastic moduli for the corresponding crystal. The model does not take into account the formation of a Si–Li alloy due to the formation of chemical bonds. A more accurate description of Si–Li interaction could be achieved using first-principle calculations. However, it is very problematic to perform

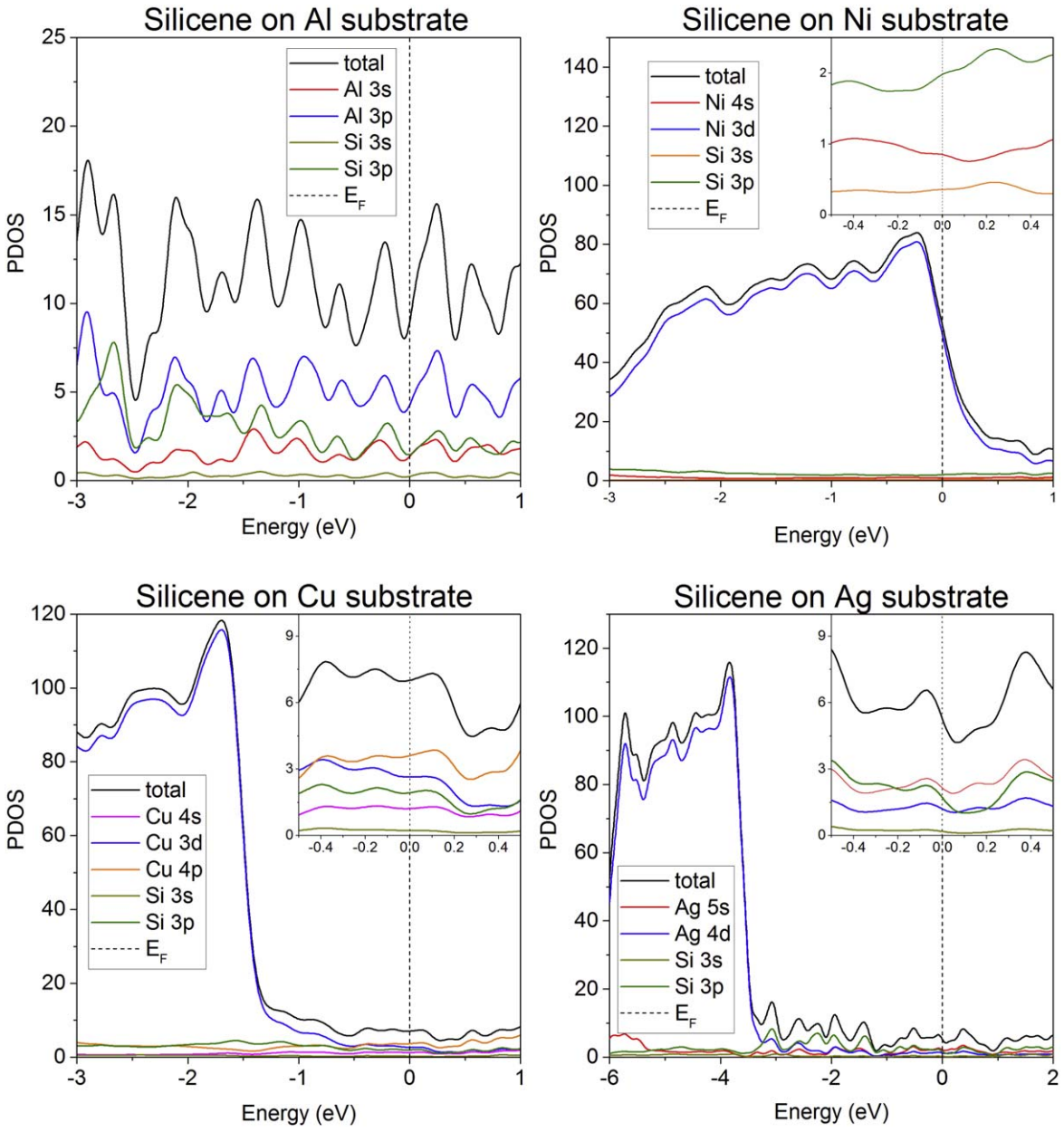

Figure 9. Partial spectra of electronic states of the systems "single-layer silicene-metal (Al, Ni, Cu, Ag) substrate." The spectra of the density of states of silicene on Ni, Cu, and Ag substrates for the conduction band at an enlarged scale are shown in the insets to the corresponding figures.

the volume of calculations performed in this study using the highly expensive ab initio molecular dynamics method.

Conclusions

The processes of intercalation and deintercalation of lithium in silicene channels, including those containing defects, and located on four different metal substrates, were studied. The highest channel occupancy with lithium was achieved when it was on a nickel and copper substrate, and the defects were mono and bivacancies, respectively. Significant fluctuations are observed in the dependence of the self-diffusion coefficient of lithium atoms on the channel occupancy with this metal. The nature of this dependence is largely determined by the type of defects present in the sheets of silicene. The stresses normal to the channel walls are decisive when filling the channel with lithium. When moving along the "chair" direction, the highest values of such local stresses appear when the channel is on a copper substrate, and the lowest—when the channel is located on an aluminum substrate. A significant part of lithium atoms intercalated into the channel is located above the centers of hexagonal rings formed by Si atoms. This creates a certain degree of crystallinity in lithium packings. The crystallinity of the packing manifests itself in regular narrow peaks of the angular distribution of the nearest geometric neighbors. The crystallinity of the packing of lithium atoms in the channel is most strongly reflected in the θ spectra for the channel on the silver substrate, and the minimum crystallinity is created in the lithium packing when the channel is on the copper substrate. Defective silicene channels on Ni (111) and Cu (111) substrates give the highest occupancy with lithium. According to the assessment, the charge capacity of a freestanding two-layer silicene during intercalation of lithium can reach 1384 mAh/g. A silicene sheet on each of the studied crystalline substrates acquires metallic conductivity. The silicene anode has a higher charge storage capacity and, therefore, has an energy density that exceeds the corresponding characteristic of the graphite anode currently in operation. Therefore, the use of silicene as the anode material can significantly increase the efficiency of LiBs.

Thus, the performed study shows that silicene can be a promising material for building the anode of a new generation of lithium-ion batteries.

Acknowledgments

This work was supported by the Russian Science Foundation [the grant number 16–13–00061].

References

1. H. Sahaf, L. Masson, C. Le'andri, B. Aufray, G. Le Lay, and F. Ronci, *Appl. Phys. Lett.*, **90**, 263110 (2007).
2. A. Fleurence, R. Friedlein, T. Ozaki, H. Kawai, Y. Wang, and Y. Yamada-Takamura, *Phys. Rev. Lett.*, **108**, 245501 (2012).
3. L. Meng et al., *Nano Lett.*, **13**, 685 (2013).
4. T. Aizawa, S. Suehara, and S. Otani, *J. Phys. Chem. C*, **118**, 23049 (2014).
5. P. De Padova, C. Quaresima, P. Perfetti, B. Olivieri, B. Le'andri, B. Aufray, S. Vizzini, and G. Le Lay, *Nano Lett.*, **8**, 271 (2008).
6. S. S. Cahangirov, M. Topsakal, E. Aktu¨rk, H. S'ahin, and S. Ciraci, *Phys. Rev. Lett.*, **102**, 236804 (2009).
7. A. Y. Galashev and K. A. Ivanichkina, *J. Electrochem. Soc.*, **165**, A1788 (2018).
8. Y.-S. Choi, J.-H. Park, J.-P. Ahn, and J.-C. Lee, *Sci. Rep.*, **7**, 14028 (2017).
9. M. Pharr, K. Zhao, X. Wang, Z. Suo, and J. J. Vlassak, *Nano Lett.*, **12**, 5039 (2012).
10. K. Persson, V. A. Sethuraman, L. J. Hardwick, Y. Hinuma, Y. S. Meng, A. van der Ven, V. Srinivasan, R. Kostecki, and G. Ceder, *J. Phys. Chem. Lett.*, **1**, 1176 (2010).
11. W. Zhang, D. Wang, and W. Zheng, *J. Energy Chem.*, **41**, 100 (2020).
12. W. Zhang, W. Zheng, X. Cui, T. Rojo, and Q. Zhang, *Adv. Sci.*, **4**, 1600168 (2017).
13. A. Y. Galashev and K. A. Ivanichkina, *Chem. Electro. Chem.*, **6**, 1525 (2019).
14. A. E. Galashev, O. R. Rakhmanova, and K. A. Ivanichkina, *J. Struct. Chem.*, **59**, 877 (2018).
15. A. Y. Galashev and K. A. Ivanichkina, *Phys. Lett. A*, **381**, 3079 (2017).
16. A. Y. Galashev and K. A. Ivanichkina, *PCCP*, **21**, 12310 (2019).
17. W. Zhang, D. Wang, and W. Zheng, *Electrochem. Energy Rev.*, **2**, 574 (2019).
18. A. M. Nolan, Y. Liu, and Y. Mo, *ACS Energy Lett.*, **4**, 2444 (2019).
19. M. N. Volochaev, Y. E. Kalinin, M. A. Kashirin, V. A. Makagonov, S. Y. Pankov, and V. V. Bassarab, *Semiconductors*, **53**, 1465 (2019).
20. J. Tersoff, *Phys. Rev. B: Condens. Matter*, **39**, 5566 (1989).
21. S. M. Foiles, M. I. Baskes, and M. S. Daw, *Phys. Rev. B*, **33**, 7983 (1986).
22. R. Yu, P. Zhai, G. Li, and L. Liu, *J. Electron. Mater.*, **41**, 1465 (2012).
23. K.-N. Chiang, C.-Y. Chou, C.-J. Wu, C.-J. Huang, and M.-C. Yew, in *ICCES* (Institute of Electrical and Electronics Engineers (IEEE), Cairo, Egypt) 9, 130 (2009), ICCESISBN 9781424458424.
24. S. K. Das, D. Roy, and S. Sengupta, *J. Phys. F: Metal. Phys.*, **7**, 5 (1977).
25. A. Y. Galashev, *Comp. Mater. Sci.*, **98**, 123 (2015).
26. A. E. Galashev, Y. P. Zaikov, and R. G. Vladykin, *Rus. J. Electrochem.*, **52**, 966 (2016).
27. A. E. Galashev, K. A. Ivanichkina, A. S. Vorob′ev, and O. R. Rakhmanova, *Phys. Solid State*, **59**, 1242 (2017).
28. Q.-X. Pei, Z.-D. Sha, Y.-Y. Zhang, and Y.-W. Zhang, *J. Appl. Phys.*, **115**, 023519 (2014).
29. P. Ordejon, E. Artacho, and J. M. Soler, *Phys. Rev. B*, **53**, 10441 (1996).
30. P. Hohenberg and W. Kohn, *Phys. Rev. B*, **136**, 864 (1964).
31. P. E. Bloechl, *Phys. Rev. B: Condens. Mater.*, **50**, 17953 (1994).
32. J. P. Perdew, K. Burke, and M. Ernzerhof, *Phys. Rev. Lett.*, **77**, 3865 (1996).
33. A. Y. Galashev and A. S. Vorob'ev, *J. Solid State Electrochem.*, **22**, 3383 (2018).
34. S. Xu, X. Fan, J. Liu, D. J. Singh, Q. Jiang, and W. Zheng, *PCCP*, **20**, 8887 (2018).
35. S. Plimpton, *J. Comp. Phys.*, **117**, 1 (1995).
36. R. Quhe, Y. Yuan, J. Zheng, Y. Wang, Z. Ni, J. Shi, D. Yu, J. Yang, and J. Lu, *Sci. Rep.*, **4**, 5476 (2014).
37. J. Gao and J. Zhao, *Sci. Rep.*, **2**, 861 (2012).
38. V. Chevrier and J. Dahn, *J. Electrochem. Soc.*, **156**, A454 (2009).
39. X. Tan, C. R. Cabrera, and Z. Chen, *J. Phys. Chem. C*, **118**, 25836 (2014).
40. J. Wintterlin and M. L. Bocquet, *Surf. Sci.*, **603**, 1841 (2009).
41. A. V. Generalov, E. N. Voloshina, and Y. S. Dedkov, *Appl. Surf. Sci.*, **267**, 8 (2013).
42. J. Zheng, Y. Wang, L. Wang, R. Quhe, Z. Ni, W.-N. Mei, Z. Gao, D. Yu, J. Shi, and J. Lu, *Sci. Rep.*, **3**, 2081 (2013).
43. A. M. Shikin, V. K. Adamchuk, and K. H. Rieder, *Phys. Solid State*, **51**, 2390 (2009).
44. G. Le Lay, B. Aufray, C. Leandri, H. Oughaddou, J.-P. Biberian, P. De Padova, M. E. Davila, B. Ealet, and A. Kara, *Appl. Surf. Sci.*, **256**, 524 (2010).
45. Y. Fukaya, I. Mochizuki, W. Maekawa, K. Wada, T. Hyodo, I. Matsuda, and A. Kawasuso, *Phys. Rev. B*, **88**, 205413 (2013).
46. A. Acun, B. Poelsema, H. Zandvliet, and R. van Gastel, *Appl. Phys. Lett.*, **103**, 263119 (2013).
47. A. Y. Galashev and Y. P. Zaikov, *J. Appl. Elecrtochem.*, **49**, 1027 (2019).
48. A. P. Bartok, J. Kermode, N. Bernstain, and G. Csanyi, *Phys. Rev. X*, **8**, 041048 (2018).